



# Mixed Convection in MHD Second Grade Nanofluid Flow Through a Porous Medium Containing Nanoparticles and Gyrotactic Microorganisms with Chemical Reaction

Noor Saeed Khan<sup>a</sup>

<sup>a</sup>Department of Mathematics, Abdul Wali Khan University, Mardan, 23200, Khyber Pakhtunkhwa, Pakistan

**Abstract.** Mixed convection in magnetohydrodynamic second grade nanofluid flow through a porous medium containing nanoparticles and gyrotactic microorganisms with chemical reaction is considered. Buongiorno's nanofluid model is used incorporating the buoyancy forces and Darcy-Forchheimer effect. Nanoparticles increase the thermal conduction in bioconvection flow and microorganisms simultaneously increase the stability of nanofluids. For the constructive (or generation) chemical reaction, the mass transfer displays an increasing behavior. Ordinary differential equations together with the boundary conditions are obtained through the similarity variables from the governing equations of the problem, which are solved by the Homotopy Analysis Method (HAM). The investigations are presented through graphs and the results are interpreted which depict the influences of all the embedded parameters.

## 1. Introduction

Bio-convection is a natural phenomenon obtained by randomly moving of microorganisms in single-celled or in a colony of cells form. Different bio-convection systems are exist due to the motion in particular direction of the multiple types of microorganisms. Gyrotactic microorganisms move against the gravity in still fluid while their up swimming is made denser in the upper part of the suspension than the lower part. Mixed convection has applications in biofuel, fertilizers, ethanol, enzyme bio-sensors, biotechnology and various environmental systems. Khan *et al.* [1] reported the comparison of Casson and Williamson nanofluids flow containing nanoparticles and gyrotactic microorganisms using actively controlled nanofluid model boundary conditions. Their results show that stratification is dependent on microorganisms concentration. Amirson *et al.* [2] presented the three-dimensional flow of bio-convection nanofluids containing gyrotactic microorganisms past a bi-axial stretching sheet with the effects of anisotropic slip, thermal jump and mass slip. Waqas *et al.* [3] investigated the modified second-grade nanofluid flow and heat transfer with nanoparticles concentration and motile microorganisms past a stretching surface exploring the rheological behavior. Khan *et al.* [4] analyzed the bioconvection flow of Oldroyd-B nanofluid past a periodically moving stretching sheet under the effective Prandtl number. Mansour *et al.* [5] investigated the mixed bioconvection in a square lid-driven cavity filled with gyrotactic microorganisms with different magnetic field inclinations

---

2010 Mathematics Subject Classification. Primary 74A15

**Keywords.** Chemical reaction; MHD; gravity-driven; second grade nanofluid; mixed convection; passively controlled nanofluid model; gyrotactic microorganisms; convective boundary conditions; homotopy analysis method.

Received: 11 November 2017; Revised: 23 December 2017; Accepted: 08 January 2018

Communicated by Maria Alessandra Ragusa

Email address: noorsaedkhan@tak@gmail.com (Noor Saeed Khan)

in which the left wall of the lid-driven cavity is moving up with a constant speed in the vertical direction. Zaman and Gul [6] reported the MHD bioconvection flow of Williamson nanomaterial in the presence of gyrotactic microorganisms with nanoparticles, buoyancy forces and Newtonian conditions. Waqas *et al.* [7] investigated the numerical study of micropolar nanofluid past the moving sheet in the presence of activation energy, microorganisms and Nield boundary conditions. Ramzan *et al.* [8] explored the flow of aqueous based nanofluid comprising single and multi-wall carbon nanotubes over a vertical cone through a porous medium with heat generation/absorption, gyrotactic microorganisms, thermal radiation, Joule heating and chemical reaction. Sohail *et al.* [9] discussed the entropy analysis of three dimensional flow of Maxwell nanofluid containing gyrotactic microorganisms in the presence of homogeneous-heterogeneous reactions with Cattaneo-Christov heat flux and mass diffusion. Some other studies on bioconvection can be read in the references [10–15].

Many engineering, biomedical and industrial processes are highly affected by magnetohydrodynamic fluid flows which are used to pump, heat levitate, stir liquid metals, designing of cooling and heating systems, instruments of blood flow measurement, nuclear reactors, MHD generators, neutrons diffusion rate regulation etc. Scientists and researchers are active to explore magnetohydrodynamics. Anjum *et al.* [16] focused to elaborate the features of entropy generation in polystyrene-water and polystyrene-kerosene nanofluids with the combined phenomena of thermal stratification and convective boundary conditions with viscous dissipation and stagnation points in the presence of MHD to analyze the flow characteristics deformed by the Riga plate. Lu *et al.* [17] elaborated the effects of magnetohydrodynamic and Cattaneo-Christov heat flux on the squeezing flow, heat and mass transfer of carbon nanotubes over two disks using *bvp4c* function of the MAPLE software. Jawad *et al.* [18] analyzed the rotational stagnation-point flow of Maxwell nanofluid past a porous radially stretching/shrinking rotating disk using Buongiorno's nanofluid model and Von Karman similarity variables. Raju *et al.* [19] examined the magnesium oxide+water and magnesium oxide+ethylene glycol nanofluid in the presence of magnetohydrodynamics to show that time taken for execution is more in magnesium oxide with ethylene glycol mixture compared to magnesium oxide+water for all the considered non-dimensional parameters. The other MHD studies can be seen in the references [20–29].

The convective heat transfer in the porous medium has extensive applications including boilers operating, heat exchangers, water filtration, oil and gas flowing in reservoirs, groundwater flows, fuel cells, transfer of drugs in tissues, packed-bed energy storage systems, fluidized beds, thermal insulation etc.

The popular Navier-Stokes equations are used to study the dynamics of fluids in permeable or impermeable medium. Scientists and researchers are investigating different types of problems using Navier-Stokes equations. There are interesting studies employing Navier-Stokes equations which can be solved through the common techniques of integration. To this end, Benbernou [30] established a Serrin-type regularity criterion in terms of pressure for Leray weak solutions to the Navier-Stokes equations. Involving fluid flow, Gala *et al.* [31] presented a study that deals with the blow-up criterion for the hydrodynamic system modeling the flow of three-dimensional nematic liquid crystal materials. In another note, Gala *et al.* [32] considered the regularity problem under the critical condition to the Boussinesq equations with zero heat conductivity. Applying Navier-Stokes equations to the physical problems, Khan *et al.* [33] discussed the behavior of flow and transfer of heat analysis of a second-grade fluid through a porous medium past a stretching sheet showing that the velocity and temperature decrease with porosity parameter. Hussain *et al.* [34] worked on a numerical study for the effect of porosity and internal heat generation/absorption on mixed convection flow of nanofluid over a backward facing step along with the entropy generation in which the channel downstream bottom wall is isothermally heated while the remaining walls of the channel are thermally insulated. Ramesh [35] examined the behavior of three different hybrid nanoparticles flow in porous medium characterized by Forchheimer medium across a rotating disk using convective conditions for heat transfer and RKF method. Gosh and Mukhopadhyay [36] presented the nanofluid flow over an exponentially porous shrinking sheet in the presence of velocity slip and thermal slip under the effects of silver nanoparticle in two different types of base fluids. Khan *et al.* [37] worked on a transient MHD flow in Carreau-Yasuda nanofluid produced by impulsively started disk in the presence of Darcy-Forchheimer and chemical reactive species considering conventional Fourier's and Fick' laws.

The authors have analyzed the mixed convection in gravity-driven MHD second grade nanofluid flow con-

taining both nanoparticles and gyrotactic microorganisms through a Darcy-Forchheimer porous medium with chemical reaction along a convectively heated vertical surface. Similarity transformations are used in the basic governing equations of the problem to convert it to dimensionless form which have been solved using a powerful analytic tool Homotopy Analysis Method (HAM) [38]. The influences of all the pertinent parameters on velocity, temperature, concentration and density motile microorganisms profiles have been shown graphically and illustrated.

## 2. Methods

### 2.1. Basic equations

A flow of MHD, unsteady, laminar and an incompressible second grade nanofluid falling downwards along a vertical solid surface due to gravity in two dimensions is under focused. The uniform downward flow on the right side of the plate has a constant temperature  $T_\infty$  at  $x = 0$  and the nanofluid on the left side of the plate has another constant temperature  $T_f$ . Darcy-Forchheimer effect is involved for the porous medium. For removing the bioconvection instability, supposition is that the nanofluid is in dilute form and the stability of the nanoparticles suspended in the base fluid exist so that the nanoparticles do not agglomerate in the fluid. There does not exist nanoparticles flux at the solid wall. It is assumed that microorganisms are constantly distributed at the wall. For the survival of the microorganisms, the base fluid is taken as water. A magnetic field of intensity  $B_0$  is imposed in the positive  $y$ -direction. The absence of applied voltage and the magnetic Reynolds make the induced magnetic field and Hall effects too much less which can be considered to zero. The physical description of the problem is shown in Fig. 1.

Applying aforementioned suppositions, the basic governing equations are as in [1, 10, 13–15]

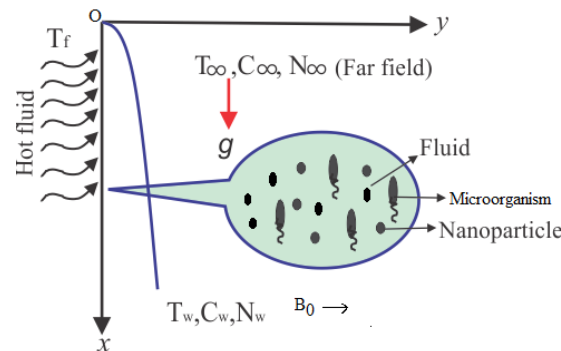


Figure 1: Problem geometry.

$$\frac{\partial u}{\partial x} + \frac{\partial v}{\partial y} = 0, \tag{1}$$

$$\rho_f \left( u \frac{\partial u}{\partial x} + v \frac{\partial u}{\partial y} \right) = \rho_f U \frac{dU}{dx} + \mu_f \frac{\partial^2 u}{\partial y^2} + \alpha_1 \left[ \frac{\partial}{\partial x} \left( u \frac{\partial^2 u}{\partial y^2} \right) - \frac{\partial u}{\partial y} \frac{\partial^2 u}{\partial x \partial y} + v \frac{\partial^3 u}{\partial y^3} \right] + \left[ (1 - C) \rho_{f_\infty} g \beta (T - T_\infty) \right] - \left[ (\rho_p - \rho_{f_\infty}) g (C - C_\infty) \right] + \left[ g (N - N_\infty) \gamma_{av} \Delta \rho \right] - \sigma B_0^2 u - \frac{\nu_f}{k} (u - U_\infty) - \frac{k^F}{\sqrt{k}} (u^2 - U_\infty^2), \tag{2}$$

$$u \frac{\partial T}{\partial x} + v \frac{\partial T}{\partial y} = \lambda \frac{\partial^2 T}{\partial y^2} + \tau \left[ D_B \left( \frac{\partial C}{\partial y} \frac{\partial T}{\partial y} \right) + \left( \frac{D_T}{T_\infty} \right) \left( \frac{\partial T}{\partial y} \right)^2 \right], \tag{3}$$

$$u \frac{\partial C}{\partial x} + v \frac{\partial C}{\partial y} = \frac{D_B \partial^2 C}{\partial y^2} + \frac{D_T}{T_\infty} \frac{\partial^2 T}{\partial y^2} - k_r(C - C_\infty), \tag{4}$$

$$u \frac{\partial N}{\partial x} + v \frac{\partial N}{\partial y} + \frac{\partial(N\tilde{v})}{\partial y} = D_n \frac{\partial^2 N}{\partial y^2}. \tag{5}$$

Here

$$\frac{dp}{dx} = \rho_f U \frac{dU}{dx}, \quad U = (2ax)^{\frac{1}{2}}, \tag{6}$$

where  $U$  represents the free stream velocity,  $a$  represents constant,  $u$  and  $v$  are the velocity components in the  $x$ - and  $y$ -directions.  $\alpha_1$  is the normal stress moduli,  $\tilde{v} = \left( \frac{bW_c}{\Delta C} \right) \nabla C$  represents the average swimming velocity vector of the oxytactic microorganisms embedding  $b$  which represents the chemotaxis constant and  $W_c$  represents the maximum cell swimming speed. The subscripts  $p$ ,  $f$  and  $f_\infty$  represent respectively the solid particles, the nanofluid and the base fluid at far field.  $\Delta\rho = \rho_{cell} - \rho_{f_\infty}$  represents the density difference between a cell and base fluid density at far field,  $\mu_f$  represents the dynamic viscosity,  $\gamma_{av}$  represents the average volume of microorganisms,  $\sigma$  represents the electrical conductivity and  $\rho_f$  represents the density of the nanofluid.  $\nu_f = \frac{\mu_f}{\rho_f}$  represents the kinematic viscosity,  $\beta$  represents the coefficient of volumetric volume expansion of a second grade nanofluid,  $g$  represents the acceleration due to gravity,  $C$  represents the nanoparticle volume fraction,  $k = k_0 x$  represents the permeability of porous medium and  $k^F = \frac{k_0^F}{\sqrt{x}}$  represents the Forchheimer resistance factor where  $k_0$  represents the initial permeability.  $N$  represents the number density of motile microorganisms,  $C_\infty$  represents the ambient nanofluid volume fraction,  $\lambda = \frac{k_1}{\rho_f}$  represents the thermal diffusivity of the nanofluid in which  $k_1$  represents the thermal conductivity,  $k_r$  represents the rate (constant) of chemical reaction,  $\tau = \frac{(\rho c)_p}{(\rho c)_f}$  represents the ratio of nanoparticle heat capacity and the base fluid heat capacity at constant pressure  $P$ ,  $D_B$  represents the Brownian diffusion coefficient at constant pressure,  $D_n$  represents the diffusivity of microorganisms,  $T_\infty$  represents the ambient temperature,  $D_T$  represents the thermophoretic diffusion coefficient and  $T$  represents the temperature inside the boundary layer.

The boundary conditions are

$$u = 0, \quad v = 0, \quad -k_1 \frac{\partial T}{\partial y} = h_f(T_f - T), \quad D_B \frac{dC}{dy} + \frac{D_T}{T_\infty} \frac{dT}{dy} = 0, \quad N = N_w \quad \text{at} \quad y = 0, \tag{7}$$

$$u \rightarrow U(x), \quad \frac{\partial u}{\partial y} \rightarrow 0, \quad T \rightarrow T_\infty, \quad C \rightarrow C_\infty, \quad N \rightarrow N_\infty \quad \text{as} \quad y \rightarrow \infty, \tag{8}$$

where  $h_f(x)$  represents the coefficient of heat transfer on behalf of  $T_f$ ,  $C_w$  represents the wall nanofluid (second grade) volume fraction,  $N_w$  represents the wall concentration of microorganisms and  $N_\infty$  represents the ambient concentration of microorganisms.  $N_\infty = 0$  so that the boundary conditions are satisfied at infinity.

Applying the transformations for nondimensional variables  $f, \theta, \phi, \Omega$  and similarity variable  $\zeta$  as

$$\psi(x, y) = \left( \frac{4U\nu_f x}{3} \right)^{\frac{1}{2}} f(\zeta), \quad \theta(\zeta) = \frac{T - T_\infty}{T_f - T_\infty}, \quad \phi = \frac{C - C_\infty}{C_w - C_\infty}, \quad \Omega = \frac{N - N_\infty}{N_w - N_\infty}, \quad \zeta = \left[ \frac{3U}{4\nu_f x} \right]^{\frac{1}{2}} y, \tag{9}$$

where  $\psi$  represents the stream function which is used as  $u = \frac{\partial\psi}{\partial y}$  and  $v = -\frac{\partial\psi}{\partial x}$ ,  $x$  and  $y$  are the Cartesian coordinates along surface and normal to it. Equation (9) identically satisfies mass conservation equation

(1). With the help of equation (9), the equations (2)-(5), (7)-(8) yield the following six equations (10)-(15).

$$f''' + \frac{2}{3}(1 - f^2) + ff'' + \gamma_1(2ff''' - f'^2 - 3ff''v) + Gr\theta - Nr\phi + Rb\Omega - Mf' - \gamma_3f' - \gamma_4f'^2 = 0, \quad (10)$$

$$\theta'' + Prf\theta' + Nt(\theta')^2 + Nb\theta'\phi' = 0, \quad (11)$$

$$\phi'' + Lef\phi' + \frac{Nt}{Nb}\theta'' - \gamma_5\phi = 0, \quad (12)$$

$$\Omega'' + Scf\Omega' + Pe(\phi'\Omega' + \phi''\Omega) = 0, \quad (13)$$

$$f = f' = 0, \quad \theta' = -\gamma_2(1 - \theta), \quad Nb\phi' + Nt\theta' = 0, \quad \Omega = 1 \quad \text{at} \quad \zeta = 0, \quad (14)$$

$$f = 1, \quad f' = 0, \quad \theta = 0, \quad \phi = 0, \quad \Omega = 0 \quad \text{at} \quad \zeta = \infty, \quad (15)$$

where  $\gamma_1 = \frac{\alpha_1 U}{4\mu_f x}$  represents the non-dimensional second grade nanofluid parameter,

$Gr = \frac{2(1 - C_\infty)\rho_{f\infty}g\beta(T_f - T_\infty)}{3a\rho_f}$  represents the buoyancy parameter (Grashof number),  $Nr = \frac{2(\rho_p - \rho_f)C_\infty g}{3a\rho_f}$  represents the buoyancy ratio parameter,  $Rb = \frac{2(N_w - N_\infty)g\gamma_w\Delta\rho}{3a\rho_f}$  represents the bioconvection Rayleigh number,  $Pr = \frac{\nu_f}{\lambda}$  represents the Prandtl number,  $Nt = \frac{\tau D_T(T_f - T_\infty)}{\lambda T_\infty}$  represents the thermophoresis parameter,  $Nb = \frac{\tau D_B C_\infty}{\lambda}$  represents the Brownian motion parameter,  $Le = \frac{\nu_f}{D_B}$  represents the Lewis number,  $Sc = \frac{\nu_f}{D_n}$  represents the Schmidt number,  $Pe = \frac{bW_c}{D_n}$  represents the bioconvection Peclet number,  $\gamma_2 = \frac{h_f}{k_1} \sqrt{\frac{4x\nu_f}{3U}}$  represents the reduced heat transfer parameter,  $\gamma_3 = \frac{4\nu_f}{3k_0 U}$  represents the porosity parameter and  $\gamma_4 = \frac{4k_f^F}{3\sqrt{k_0}}$  represents the inertial parameter,  $\gamma_5 = \frac{k_r(C_w - C_\infty)}{\lambda}$  represents the chemical reaction parameter and  $M = \frac{4\sigma B_0^2}{3\rho_f U} \sqrt{\frac{x}{2a}}$  represents the magnetic field parameter. For  $\gamma_1 = 0$ , the present study corresponds to viscous nanofluid case and if  $\gamma_1 = \gamma_3 = \gamma_4 = \gamma_5 = M = 0$ , then the non-Newtonian, Darcy Forchheimer, chemical reaction and magnetic field effects are not exist.

### 3. Solution of the Problem by Homotopy Analysis Method

Choosing the suitable initial approximations to satisfy the boundary conditions and auxiliary linear operators for velocity, temperature, concentration and motile microorganism concentration in the following form

$$f_0(\zeta) = \zeta - [\exp(-\zeta) - \exp(-2\zeta)], \quad \theta_0(\zeta) = \exp(-\zeta) - \frac{\exp(-2\zeta)}{2 + \gamma_2}, \quad \phi_0(\zeta) = -\frac{Nt\gamma_2}{Nb(\gamma_2 + 2)} \exp(-\zeta), \quad \Omega_0(\zeta) = \exp(-\zeta), \quad (16)$$

$$L_f = f''' - f', \quad L_\theta = \theta'' - \theta, \quad L_\phi = \phi'' - \phi, \quad L_\Omega = \Omega'' - \Omega. \quad (17)$$

The following properties are satisfied with the linear operators

$$L_f [C_1 + C_2 \exp(\zeta) + C_3 \exp(-\zeta)] = 0, \quad L_\theta [C_4 \exp(\zeta) + C_5 \exp(-\zeta)] = 0, \quad L_\phi [C_6 \exp(\zeta) + C_7 \exp(-\zeta)] = 0, \quad L_\Omega [C_8 \exp(\zeta) + C_9 \exp(-\zeta)] = 0, \quad (18)$$

where  $C_i (i = 1-9)$  are the arbitrary constants.

3.1. Zeroth-order deformation problems

Introducing the nonlinear operator  $\mathfrak{N}$  as

$$\begin{aligned} \mathfrak{N}_f[f(\zeta, p), \theta(\zeta, p), \phi(\zeta, p), \Omega(\zeta, p)] = & \frac{\partial^3 f(\zeta, p)}{\partial \zeta^3} + \frac{2}{3} \left[ 1 - \left( \frac{\partial f(\zeta, p)}{\partial \zeta} \right)^2 \right] + f(\zeta, p) \frac{\partial^2 f(\zeta, p)}{\partial \zeta^2} + \\ & \gamma_1 \left[ 2 \frac{\partial f(\zeta, p)}{\partial \zeta} \frac{\partial^3 f(\zeta, p)}{\partial \zeta^3} - \left( \frac{\partial^2 f(\zeta, p)}{\partial \zeta^2} \right)^2 - 3f(\zeta, p) \frac{\partial^4 f(\zeta, p)}{\partial \zeta^4} \right] + Gr\theta(\zeta, p) - Nr\phi(\zeta, p) + Rb\Omega(\zeta, p) - M \frac{\partial f(\zeta, p)}{\partial \zeta} - \\ & \gamma_3 \frac{\partial f(\zeta, p)}{\partial \zeta} - \gamma_4 \left( \frac{\partial f(\zeta, p)}{\partial \zeta} \right)^2, \end{aligned} \quad (19)$$

$$\mathfrak{N}_\theta[f(\zeta, p), \theta(\zeta, p), \phi(\zeta, p)] = \frac{\partial^2 \theta(\zeta, p)}{\partial \zeta^2} + Prf(\zeta, p) \frac{\partial \theta(\zeta, p)}{\partial \zeta} + Nt \left( \frac{\partial \theta(\zeta, p)}{\partial \zeta} \right)^2 + Nb \frac{\partial \theta(\zeta, p)}{\partial \zeta} \frac{\partial \phi(\zeta, p)}{\partial \zeta}, \quad (20)$$

$$\mathfrak{N}_\phi[f(\zeta, p), \theta(\zeta, p), \phi(\zeta, p)] = \frac{\partial^2 \phi(\zeta, p)}{\partial \zeta^2} + Lef(\zeta, p) \frac{\partial \phi(\zeta, p)}{\partial \zeta} + \frac{Nt}{Nb} \frac{\partial^2 \theta(\zeta, p)}{\partial \zeta^2} - \gamma_5 \phi(\zeta, p), \quad (21)$$

$$\mathfrak{N}_\Omega[f(\zeta, p), \phi(\zeta, p), \Omega(\zeta, p)] = \frac{\partial^2 \Omega(\zeta, p)}{\partial \zeta^2} + Scf(\zeta, p) \frac{\partial \Omega(\zeta, p)}{\partial \zeta} + Pe \left[ \frac{\partial \phi(\zeta, p)}{\partial \zeta} \frac{\partial \Omega(\zeta, p)}{\partial \zeta} + \frac{\partial^2 \phi(\zeta, p)}{\partial \zeta^2} \Omega(\zeta, p) \right], \quad (22)$$

where  $p$  is an embedding parameter such that  $p \in [0, 1]$ .

The zeroth-order deformation problems are

$$(1 - p)L_f[f(\zeta, p) - f_0(\zeta)] = p\hbar \mathfrak{N}_f[f(\zeta, p), \theta(\zeta, p), \phi(\zeta, p), \Omega(\zeta, p)], \quad (23)$$

$$(1 - p)L_\theta[\theta(\zeta, p) - \theta_0(\zeta)] = p\hbar \mathfrak{N}_\theta[f(\zeta, p), \theta(\zeta, p), \phi(\zeta, p)], \quad (24)$$

$$(1 - p)L_\phi[\phi(\zeta, p) - \phi_0(\zeta)] = p\hbar \mathfrak{N}_\phi[f(\zeta, p), \theta(\zeta, p), \phi(\zeta, p)], \quad (25)$$

$$(1 - p)L_\Omega[\Omega(\zeta, p) - \Omega_0(\zeta)] = p\hbar \mathfrak{N}_\Omega[f(\zeta, p), \phi(\zeta, p), \Omega(\zeta, p)], \quad (26)$$

where  $\hbar$  represents the auxiliary non-zero parameter.

Let us suppose that equation (23) has the boundary conditions

$$f(0, p) = 0, \quad f'(0, p) = 0, \quad f'(\infty, p) = 1. \quad (27)$$

Equation (24) has the boundary conditions

$$\theta'(0, p) = -\gamma_2(1 - \theta(0, p)), \quad \theta(\infty, p) = 0. \quad (28)$$

Equation (25) has the boundary conditions

$$Nb\phi'(0, p) + Nt\theta'(0, p) = 0, \quad \phi(\infty, p) = 0. \quad (29)$$

Similarly equation (26) has the boundary conditions

$$\Omega(0, p) = 1, \quad \Omega(\infty, p) = 0. \quad (30)$$

For  $p = 0$  and  $p = 1$ , one obtains the following results

$$p = 0 \Rightarrow f(\zeta, 0) = f_0(\zeta) \quad \text{and} \quad p = 1 \Rightarrow f(\zeta, 1) = f(\zeta), \quad (31)$$

$$p = 0 \Rightarrow \theta(\zeta, 0) = \theta_0(\zeta) \quad \text{and} \quad p = 1 \Rightarrow \theta(\zeta, 1) = \theta(\zeta), \quad (32)$$

$$p = 0 \Rightarrow \phi(\zeta, 0) = \phi_0(\zeta) \quad \text{and} \quad p = 1 \Rightarrow \phi(\zeta, 1) = \phi(\zeta), \quad (33)$$

Similarly

$$p = 0 \Rightarrow \Omega(\zeta, 0) = \Omega_0(\zeta) \quad \text{and} \quad p = 1 \Rightarrow \Omega(\zeta, 1) = \Omega(\zeta). \tag{34}$$

On the application of Taylor series expansion on equations (31)-(34), the simplified equations take the following forms

$$f(\zeta, p) = f_0(\zeta) + \sum_{m=1}^{\infty} f_m(\zeta)p^m, \quad f_m(\zeta) = \frac{1}{m!} \frac{\partial^m f(\zeta, p)}{\partial p^m} \Big|_{p=0}, \tag{35}$$

$$\theta(\zeta, p) = \theta_0(\zeta) + \sum_{m=1}^{\infty} \theta_m(\zeta)p^m, \quad \theta_m(\zeta) = \frac{1}{m!} \frac{\partial^m \theta(\zeta, p)}{\partial p^m} \Big|_{p=0}, \tag{36}$$

$$\phi(\zeta, p) = \phi_0(\zeta) + \sum_{m=1}^{\infty} \phi_m(\zeta)p^m, \quad \phi_m(\zeta) = \frac{1}{m!} \frac{\partial^m \phi(\zeta, p)}{\partial p^m} \Big|_{p=0}, \tag{37}$$

$$\Omega(\zeta, p) = \Omega_0(\zeta) + \sum_{m=1}^{\infty} \Omega_m(\zeta)p^m, \quad \Omega_m(\zeta) = \frac{1}{m!} \frac{\partial^m \Omega(\zeta, p)}{\partial p^m} \Big|_{p=0}. \tag{38}$$

The convergence of the series is sharply relying on  $\hbar$ . Suppose  $\hbar$  is taken in such a manner that the series in equations (35)-(38) converge at  $p = 1$ , then equations (35)-(38) result in

$$f(\zeta) = f_0(\zeta) + \sum_{m=1}^{\infty} f_m(\zeta), \tag{39}$$

$$\theta(\zeta) = \theta_0(\zeta) + \sum_{m=1}^{\infty} \theta_m(\zeta), \tag{40}$$

$$\phi(\zeta) = \phi_0(\zeta) + \sum_{m=1}^{\infty} \phi_m(\zeta), \tag{41}$$

$$\Omega(\zeta) = \Omega_0(\zeta) + \sum_{m=1}^{\infty} \Omega_m(\zeta). \tag{42}$$

### 3.2. $m$ -th order deformation problems

Operating for  $m$  times derivative with respect to  $p$  of equations (23) and (27), then dividing by  $m!$  and using  $p = 0$  provide the following equations

$$L_f[f_m(\zeta) - \chi_m f_{m-1}(\zeta)] = \hbar \mathfrak{R}_m^f(\zeta), \tag{43}$$

$$f_m(0) = f'_m(0) = f'_m(\infty) = 0, \tag{44}$$

$$\begin{aligned} \mathfrak{R}_m^f(\zeta) = f'''_{m-1} + \frac{2}{3} - \frac{2}{3} \sum_{k=0}^{m-1} [f'_{m-1-k} f'_k] + \sum_{k=0}^{m-1} [f_{m-1-k} f''_k] + \gamma_1 \sum_{k=0}^{m-1} [2f'_{m-1-k} f'''_k - f''_{m-1-k} f''_k - 3f_{m-1-k} f^{iv}_k] + \\ Gr\theta_{m-1} - Nr\phi_{m-1} + Rb\Omega_{m-1} - Mf'_{m-1} - \gamma_3 f'_{m-1} - \gamma_4 f'_{m-1-k} f'_k. \end{aligned} \tag{45}$$

Operating for  $m$  times derivative with respect to  $p$  of equations (24) and (28), then dividing by  $m!$  and using  $p = 0$  provide the following equations

$$L_\theta[\theta_m(\zeta) - \chi_m \theta_{m-1}(\zeta)] = \hbar \mathfrak{R}_m^\theta(\zeta), \tag{46}$$

$$\theta'_m(0) - \gamma_2\theta_m(0) = 0, \quad \theta_m(\infty) = 0, \tag{47}$$

$$\mathfrak{R}_m^\theta(\zeta) = \theta''_{m-1} + Pr \sum_{k=0}^{m-1} f_{m-1-k}\theta'_k + Nt \sum_{k=0}^{m-1} \theta'_{m-1-k}\theta'_k + Nb \sum_{k=0}^{m-1} \theta'_{m-1-k}\phi'_k. \tag{48}$$

Operating for  $m$  times derivative with respect to  $p$  of equations (25) and (29), then dividing by  $m!$  and using  $p = 0$  provide the following equations

$$L_\phi[\phi_m(\zeta) - \chi_m\phi_{m-1}(\zeta)] = \hbar\mathfrak{R}_m^\phi(\zeta), \tag{49}$$

$$Nb\phi'_m(0) + Nt\theta'_m(0) = \phi_m(\infty) = 0, \tag{50}$$

$$\mathfrak{R}_m^\phi(\zeta) = \phi''_{m-1} + Le \sum_{k=0}^{m-1} f_{m-1-k}\phi'_k + \frac{Nt}{Nb}\theta''_{m-1} - \gamma_5\phi_{m-1}. \tag{51}$$

Operating for  $m$  times derivative with respect to  $p$  of equations (26) and (30), then diving by  $m!$  and using  $p = 0$  provide the following equations

$$L_\Omega[\Omega_m(\zeta) - \chi_m\Omega_{m-1}(\zeta)] = \hbar\mathfrak{R}_m^\Omega(\zeta), \tag{52}$$

$$\Omega_m(0) = \Omega'_m(\infty) = 0, \tag{53}$$

$$\mathfrak{R}_m^\Omega(\zeta) = \Omega''_{m-1} + Sc \sum_{k=0}^{m-1} f_{m-1-k}\Omega'_k + Pe \sum_{k=0}^{m-1} [\phi'_{m-1-k}\Omega'_k + \phi''_{m-1-k}\Omega_k], \tag{54}$$

$$\chi_m = \begin{cases} 0, & m \leq 1 \\ 1, & m > 1. \end{cases} \tag{55}$$

If  $f_m^*(\zeta)$ ,  $\theta_m^*(\zeta)$ ,  $\phi_m^*(\zeta)$  and  $\Omega_m^*(\zeta)$  are the particular solutions, then the general solutions of equations (43), (46), (49) and (52) are

$$f_m(\zeta) = f_m^*(\zeta) + C_1 + C_2 \exp(\zeta) + C_3 \exp(-\zeta), \tag{56}$$

$$\theta_m(\zeta) = \theta_m^*(\zeta) + C_4 \exp(\zeta) + C_5 \exp(-\zeta), \tag{57}$$

$$\phi_m(\zeta) = \phi_m^*(\zeta) + C_6 \exp(\zeta) + C_7 \exp(-\zeta), \tag{58}$$

$$\Omega_m(\zeta) = \Omega_m^*(\zeta) + C_8 \exp(\zeta) + C_9 \exp(-\zeta). \tag{59}$$

#### 4. Results and Discussion

The dimensionless equations (10)-(15) are computed via MATHEMATICA using HAM code. It is interesting to discuss the role of all the emerging parameters on the non-dimensional velocity profile, non-dimensional temperature profile, non-dimensional concentration profile and non-dimensional motile gyrotactic microorganisms profile  $f(\zeta)$ ,  $\theta(\zeta)$ ,  $\phi(\zeta)$  and  $\Omega(\zeta)$  respectively. The effects of embedded parameters on the velocity  $f(\zeta)$ , temperature  $\theta(\zeta)$ , concentration  $\phi(\zeta)$  and motile gyrotactic microorganisms  $\Omega(\zeta)$  fields have been plotted in Figures (6-17), (18-25), (26-35) and (36-46) respectively. The schematic diagram of the problem is demonstrated in Fig. 1. Liao [38] introduced  $\hbar$  curves for the convergence of the series solutions of the problems. Therefore, the admissible  $\hbar$ -curves for  $f(\zeta)$ ,  $\theta(\zeta)$ ,  $\phi(\zeta)$  and  $\Omega(\zeta)$  are drawn in the ranges  $-1.3 \leq \hbar \leq 0.0$ ,  $-1.8 \leq \hbar \leq 0.2$ ,  $-2.1 \leq \hbar \leq 0.1$  and  $-2.0 \leq \hbar \leq 0.0$  in Figures (2-3) and Figures (4-5) respectively.

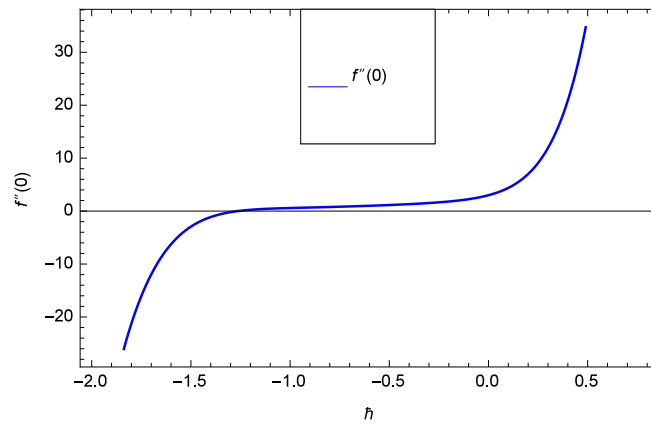


Figure 2:  $\hbar$  curve of  $f(\zeta)$ .

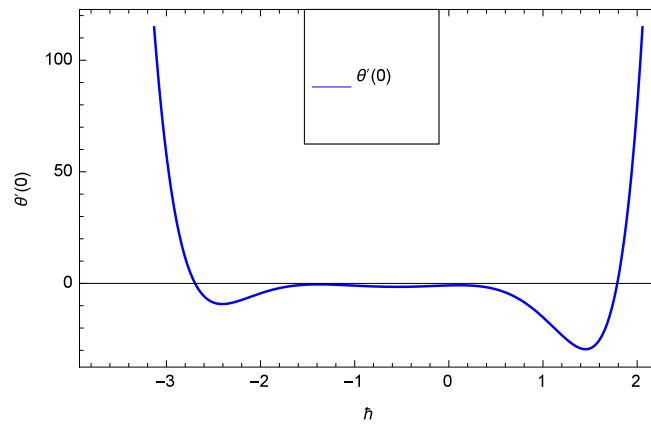


Figure 3:  $\hbar$  curve of  $\theta(\zeta)$ .

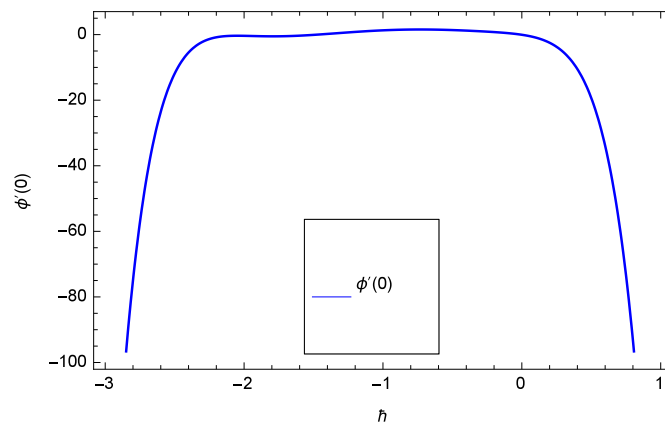


Figure 4:  $\hbar$  curve of  $\phi(\zeta)$ .

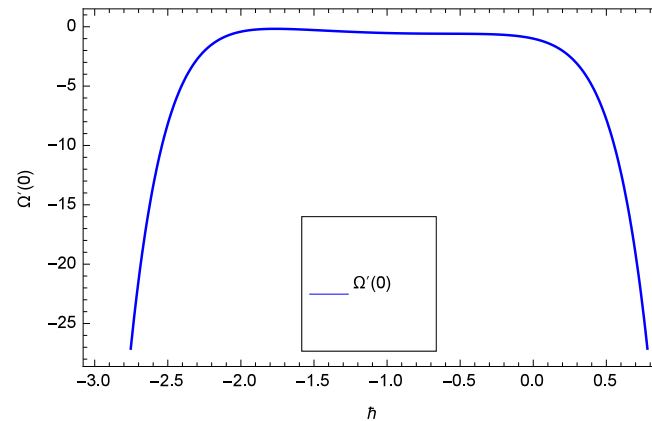


Figure 5:  $h$  curve of  $\Omega(\zeta)$ .

4.1. Velocity profile

Figure 6 presents that the motion is slow when the second grade nanofluid parameter  $\gamma_1$  increases. Figure 7 depicts that flow rises as the reduced heat transfer parameter  $\gamma_2$  rises. Figure 8 reveals that velocity  $f(\zeta)$  is completely decelerated when the porosity parameter  $\gamma_3$  is enhanced. The reason is that fluid flow receives resistivity due to porous medium holes. Figure 9 shows that motion of non-Newtonian second-grade nanofluid is reduced to minimum value as the inertial parameter  $\gamma_4$  resumes the positive values. Figure 10 projects that motion is enhanced on increasing the chemical reaction parameter  $\gamma_5$ . Gravity favors the motion with the increments in chemical reaction quantity. Figure 11 expresses that the velocity  $f(\zeta)$  rises for the rising quantities of buoyancy parameter  $Gr$ . Gravity is involved in this phenomena. Figure 12 clarifies the effect of buoyancy ratio parameter  $Nr$  on flow which has an increasing behavior. Figure 13 displays that velocity  $f(\zeta)$  has no progress for increasing quantities of bioconvection Rayleigh number  $Rb$ . Figure 14 shows that Lewis number  $Le$  accelerates the velocity  $f(\zeta)$ . Figure 15 describes that velocity  $f(\zeta)$  is made high for increasing the Schmidt number  $Sc$ . From Figure 16 it is found that the velocity  $f(\zeta)$  decreases on amplifying the values of magnetic field parameter  $M$ . Magnetic field generates Lorentz forces which retard the flow. Figure 17 provides the information about the progress of velocity  $f(\zeta)$  and Prandtl number  $Pr$ . Motion becomes fast as  $Pr$  increases.

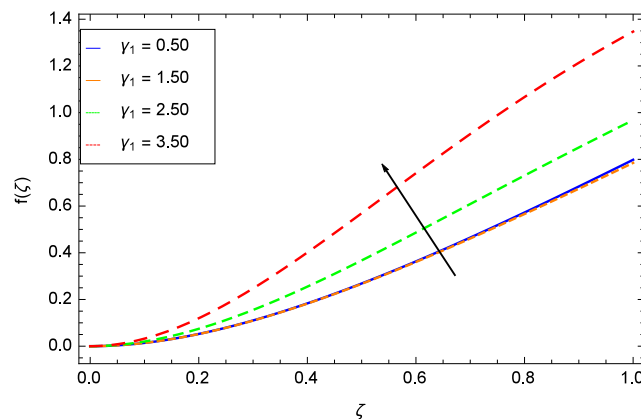


Figure 6: Role of  $f(\zeta)$  and  $\gamma_1$ .

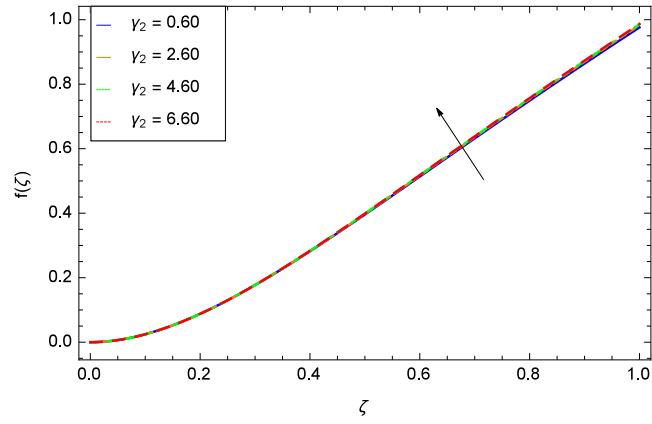


Figure 7: Role of  $f(\zeta)$  and  $\gamma_2$ .

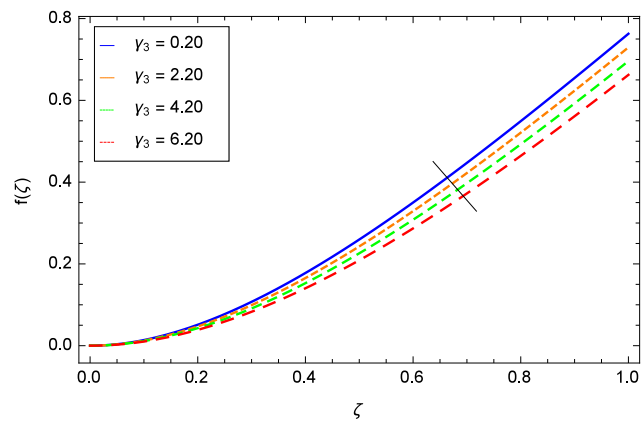


Figure 8: Role of  $f(\zeta)$  and  $\gamma_3$ .

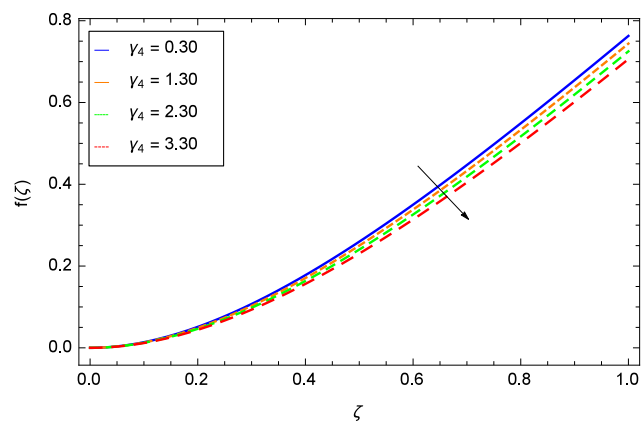


Figure 9: Role of  $f(\zeta)$  and  $\gamma_4$ .

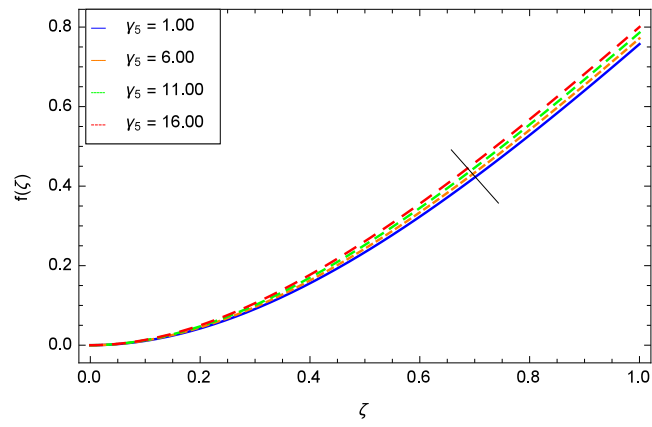


Figure 10: Role of  $f(\zeta)$  and  $\gamma_5$ .

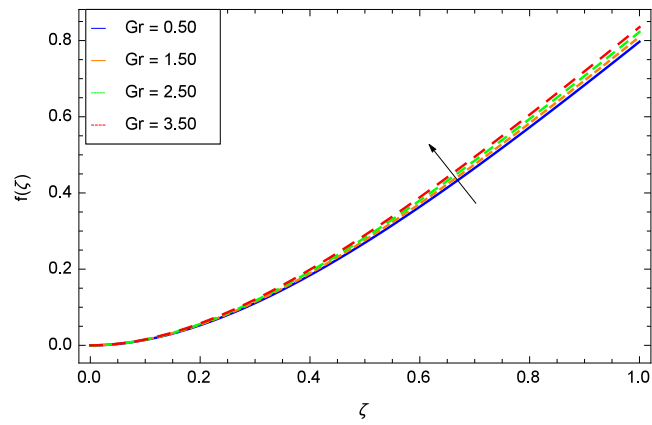


Figure 11: Role of  $f(\zeta)$  and  $Gr$ .

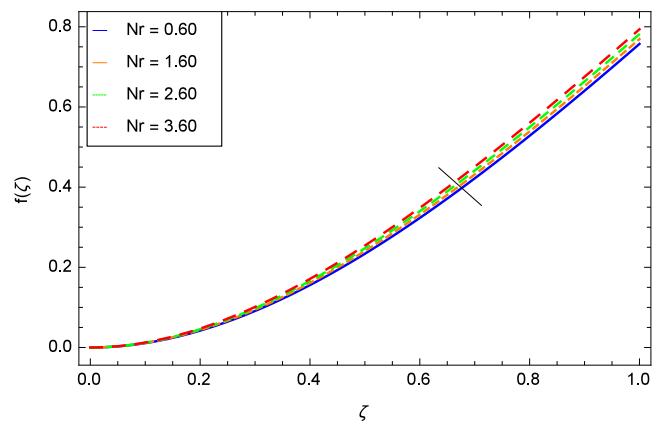


Figure 12: Role of  $f(\zeta)$  and  $Nr$ .

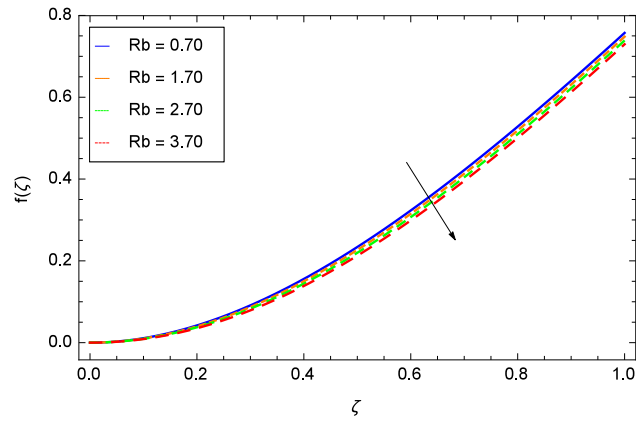


Figure 13: Role of  $f(\zeta)$  and  $Rb$ .

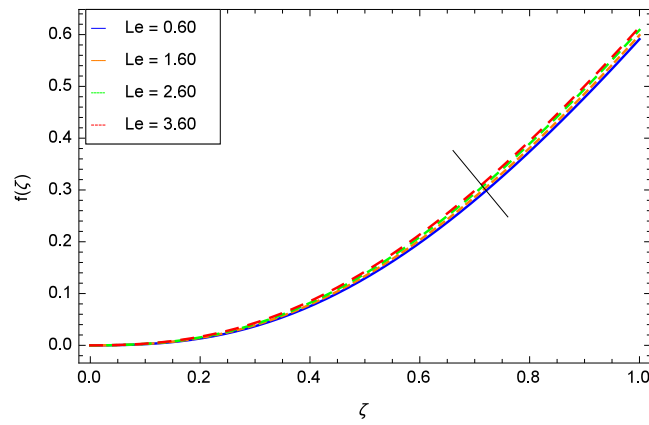


Figure 14: Role of  $f(\zeta)$  and  $Le$ .

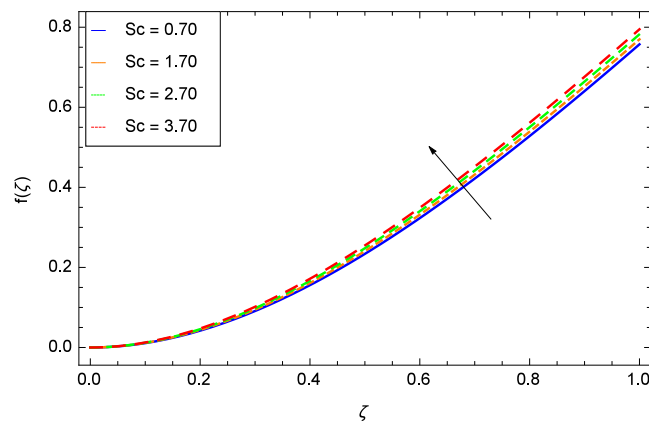


Figure 15: Role of  $f(\zeta)$  and  $Sc$ .

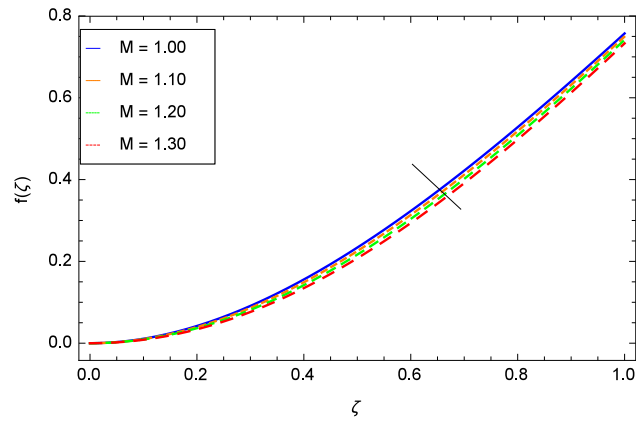


Figure 16: Role of  $f(\zeta)$  and  $M$ .

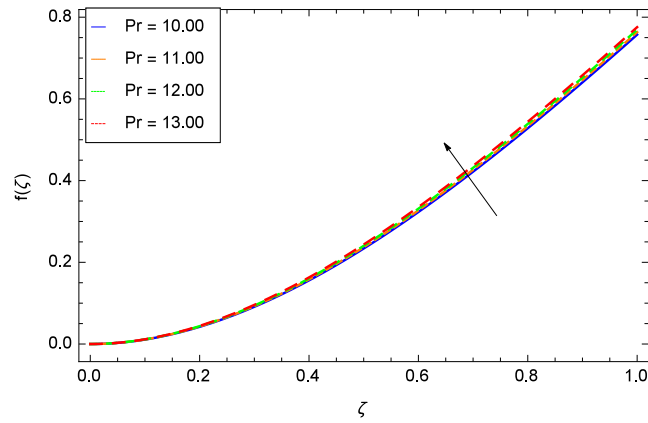


Figure 17: Role of  $f(\zeta)$  and  $Pr$ .

4.2. Temperature profile

Figure 18 exhibits that the second grade nanofluid parameter  $\gamma_1$  rises the temperature  $\theta(\zeta)$  due to viscous forces. Figure 19 demonstrates that the larger values of reduced heat transfer parameter  $\gamma_2$  mitigates the temperature  $\theta(\zeta)$ . Figure 20 reveals that the porosity parameter  $\gamma_3$  decreases the temperature since heat is used in the pores of medium. Figure 21 shows that temperature decreases as the values of inertial parameter  $\gamma_4$  increases since the medium faces resistivity on account of which heat cannot diffuse easily. Figure 22 shows that chemical reaction parameter  $\gamma_5$  increases the temperature  $\theta(\zeta)$  due to chemical combination of different species. Figure 23 displays that temperature is at once increases with the increasing values of thermophoresis parameter  $Nt$ . Magnetic field parameter  $M$  increases the temperature as shown by Figure 24. Magnetic field focuses on the controlling of heat and mass transfer flow therefore the temperature enhances for the strength of magnetic field. Prandtl number  $Pr$  makes low the temperature  $\theta(\zeta)$  as projected by Figure 25.

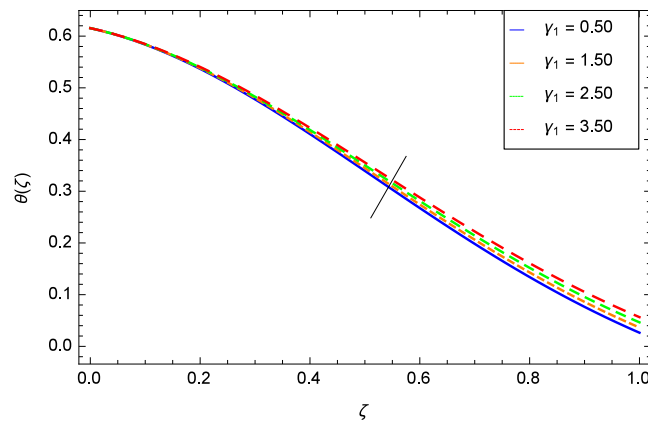


Figure 18: Role of  $\theta(\zeta)$  and  $\gamma_1$ .

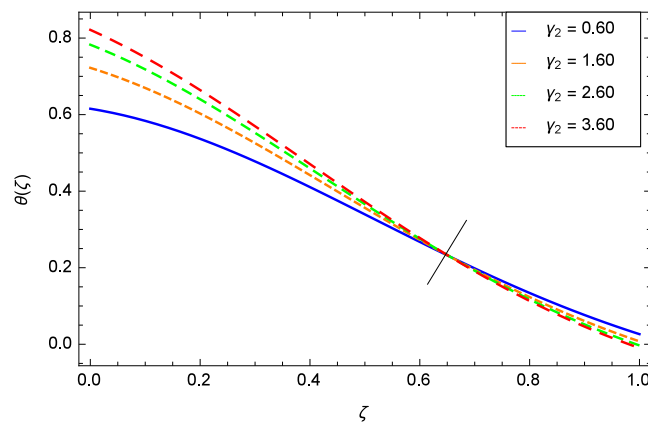


Figure 19: Role of  $\theta(\zeta)$  and  $\gamma_2$ .

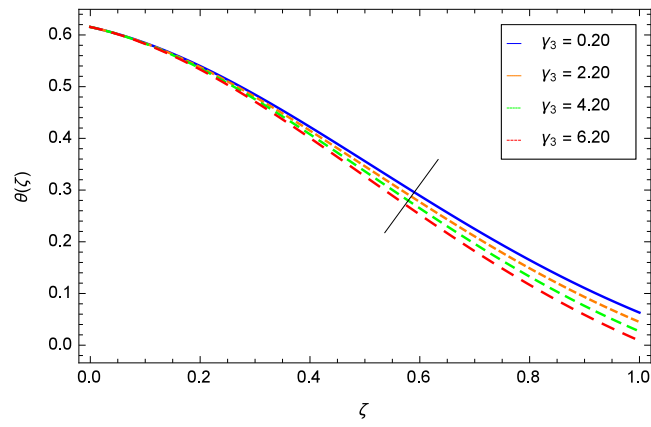


Figure 20: Role of  $\theta(\zeta)$  and  $\gamma_3$ .

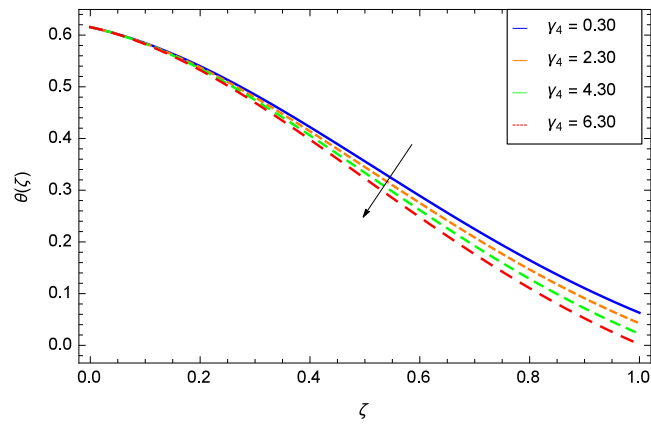


Figure 21: Role of  $\theta(\zeta)$  and  $\gamma_4$ .

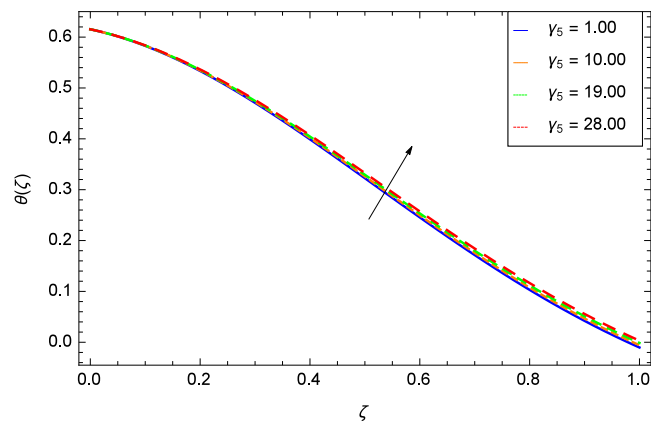


Figure 22: Role of  $\theta(\zeta)$  and  $\gamma_5$ .

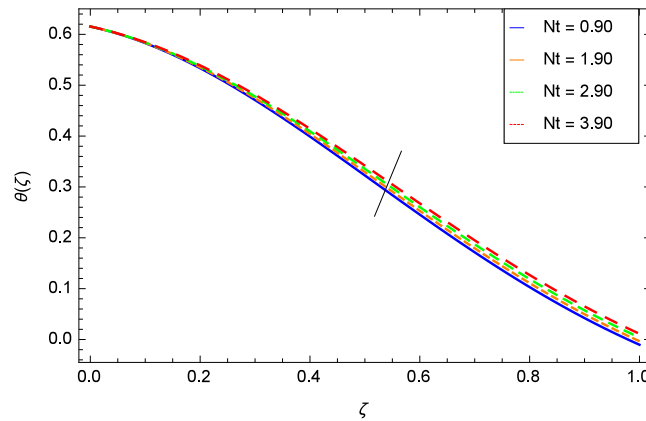


Figure 23: Role of  $\theta(\zeta)$  and  $Nt$ .

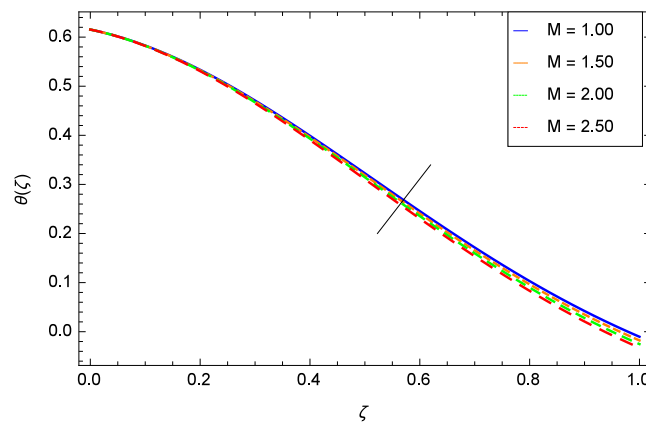


Figure 24: Role of  $\theta(\zeta)$  and  $M$ .

#### 4.3. Nanoparticles concentration profile

Figure 26 shows that the saturation becomes low with the non-Newtonian effect. As the non-Newtonian second-grade nanofluid parameter  $\gamma_1$  increases the viscous forces increase so no capacity is left for further saturation after some specific time. Figure 27 depicts that the concentration  $\phi(\zeta)$  is low for the convective heat slip parameter namely reduced heat parameter  $\gamma_2$ . The concentration rises with the greater values of porosity parameter  $\gamma_3$  which is evident from Figure 28. The inertial parameter  $\gamma_4$  increases the concentration  $\phi(\zeta)$  as shown by Figure 29. The reason is that  $\gamma_4$  basically shows the resistance which favors the nanoparticles concentration. The chemical reaction parameter  $\gamma_5$  has been enhanced the concentration depicted through Figure 30. Figure 31 shows that the Brownian motion parameter  $Nb$  increases the concentration profile  $\phi(\zeta)$ . Figure 32 specifies that the thermophoresis parameter  $Nt$  decreases the concentration profile  $\phi(\zeta)$ . Figure 33 reveals that Lewis number  $Le$  makes thick the concentration  $\phi(\zeta)$ . Figure 34 projects that the concentration field  $\phi(\zeta)$  is made strong as soon as the magnetic field parameter  $M$  is made strong. Magnetic field leads to the Lorentz force which increases the concentration. Prandtl number  $Pr$  increases the nanoparticle concentration so the  $\phi(\zeta)$  is enhanced as shown in Figure 35.

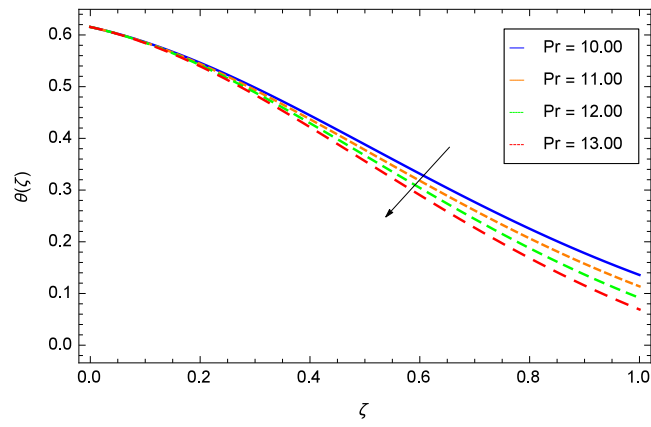


Figure 25: Role of  $\theta(\zeta)$  and  $Pr$ .

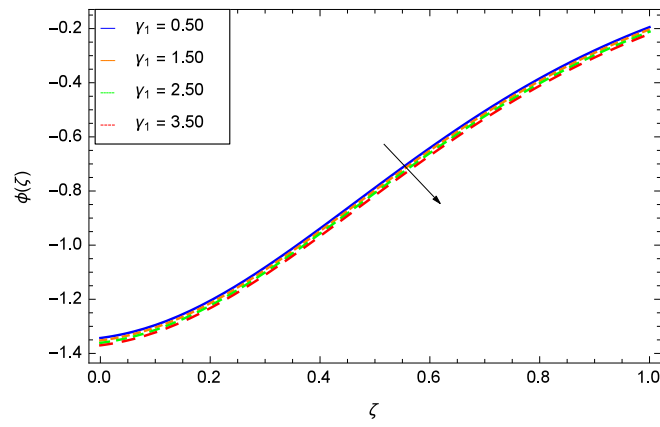


Figure 26: Role of  $\phi(\zeta)$  and  $\gamma_1$ .

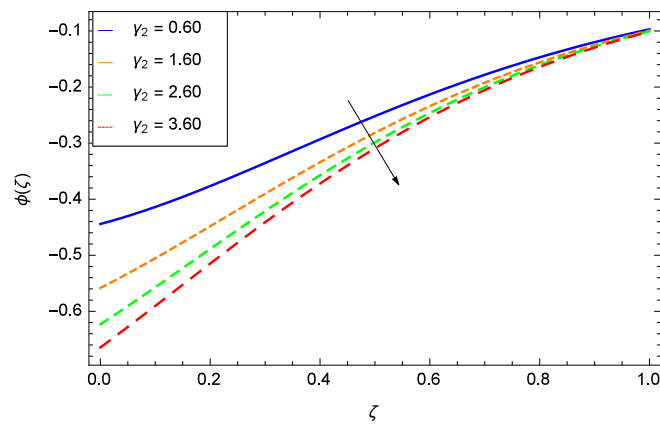


Figure 27: Role of  $\phi(\zeta)$  and  $\gamma_2$ .

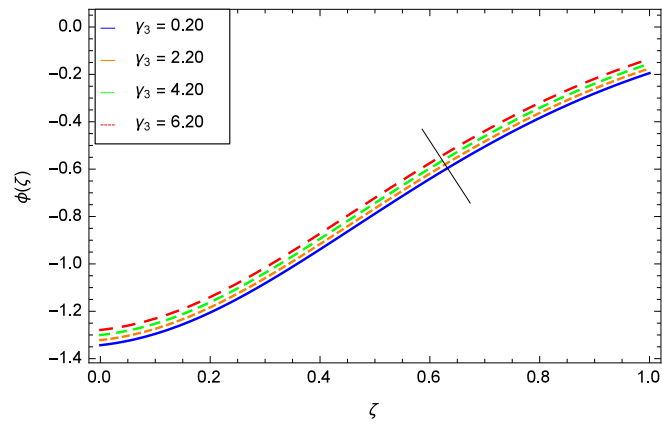


Figure 28: Role of  $\phi(\zeta)$  and  $\gamma_3$ .

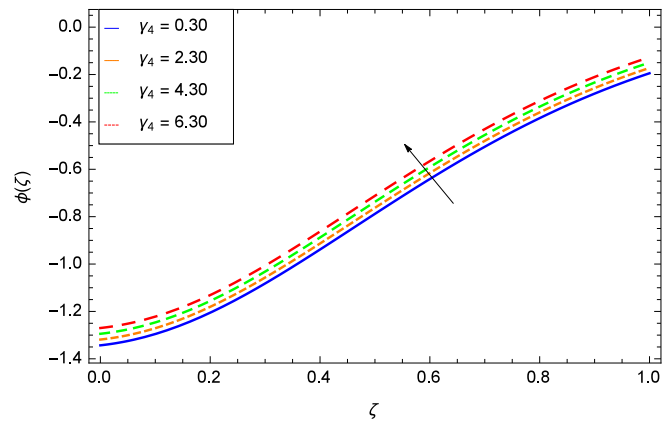


Figure 29: Role of  $\phi(\zeta)$  and  $\gamma_4$ .

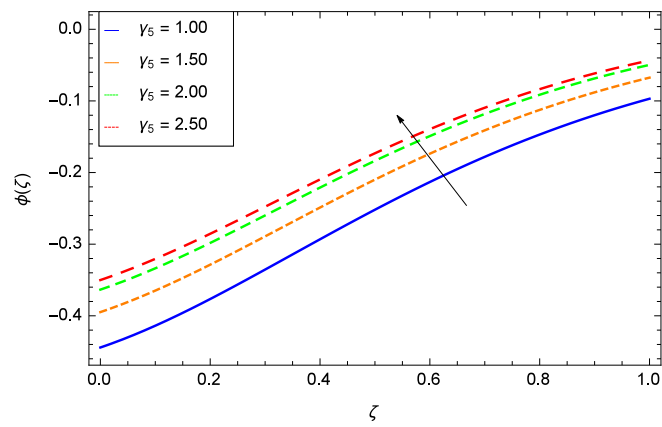


Figure 30: Role of  $\phi(\zeta)$  and  $\gamma_5$ .

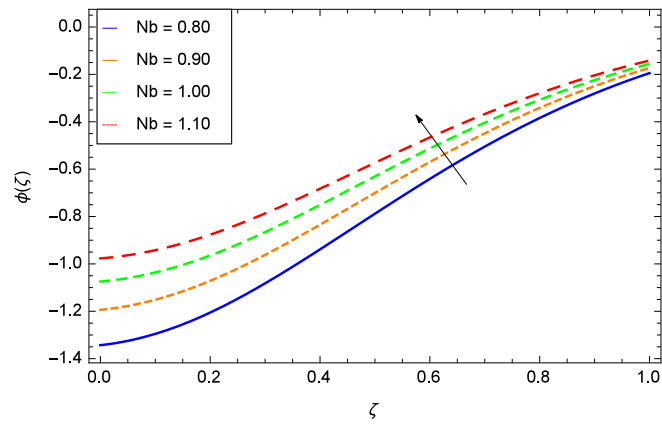


Figure 31: Role of  $\phi(\zeta)$  and  $Nb$ .

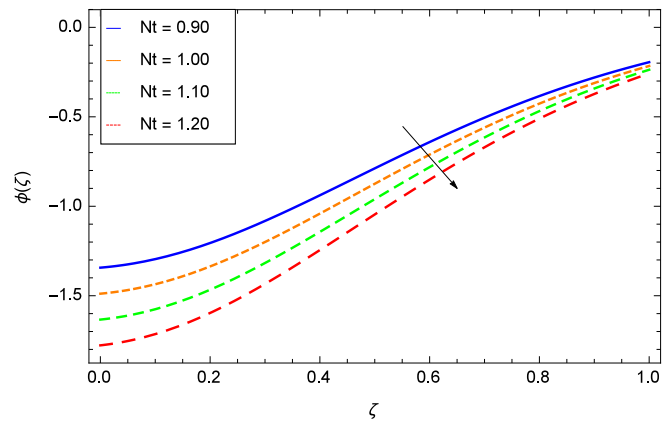


Figure 32: Role of  $\phi(\zeta)$  and  $Nt$ .

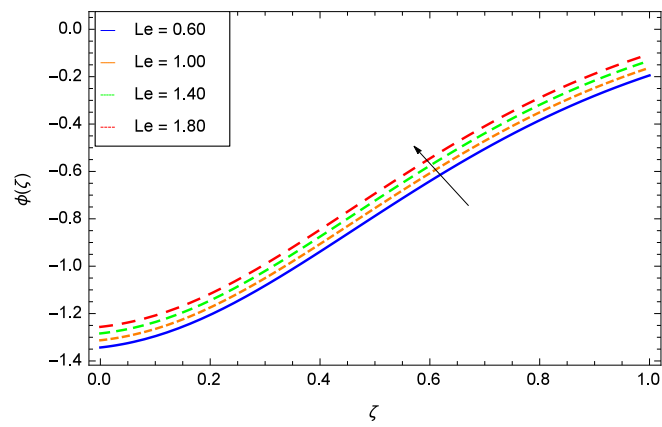


Figure 33: Role of  $\phi(\zeta)$  and  $Le$ .

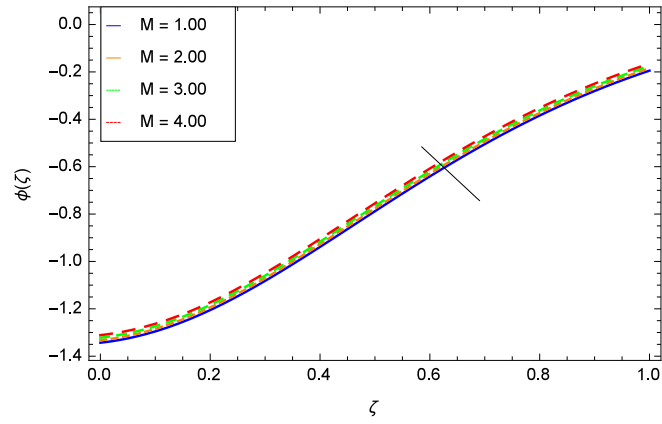


Figure 34: Role of  $\phi(\zeta)$  and  $M$ .

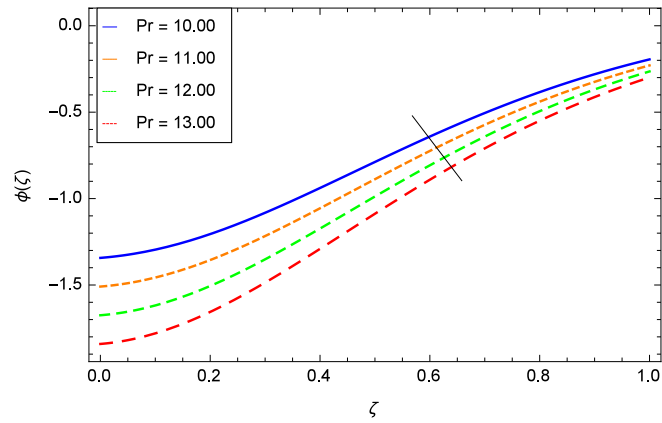


Figure 35: Role of  $\phi(\zeta)$  and  $Pr$ .

#### 4.4. Gyrotactic microorganisms concentration

Figure 36 shows that the microorganism concentration profile  $\Omega(\zeta)$  rises with larger values of second grade nanofluid parameter  $\gamma_1$ . Non-Newtonian effect has a pleasant effect on gyrotactic microorganisms. Figure 37 focuses on the role of reduced heat parameter  $\gamma_2$  on the microorganism concentration  $\Omega(\zeta)$  profile. Figure 38 shows that the microorganism concentration  $\Omega(\zeta)$  is reduced for the porosity parameter  $\gamma_3$ . The microorganisms cannot move freely in the porous medium. Figure 39 contains the non-dimensional microorganisms concentration  $\Omega(\zeta)$  profile and inertial parameter  $\gamma_4$ . The distribution of microorganisms is on low status. Figure 40 projects that the chemical reaction parameter  $\gamma_5$  increases the microorganisms concentration field  $\Omega(\zeta)$ . It is shown in Figure 41 that the microorganisms concentration  $\Omega(\zeta)$  has no progress for the Brownian motion parameter  $Nb$  due to collision of nanoparticles. Figure 42 contains the thermophoresis parameter  $Nt$  and the microorganisms concentration profile  $\Omega(\zeta)$ . Concentration is enhanced by assigning the positive values. Figure 43 illustrates that the microorganisms concentration field  $\Omega(\zeta)$  is enhanced for the greater values of Lewis number  $Le$ . Schmidt number  $Sc$  decreases the microorganisms concentration profile  $\Omega(\zeta)$  as shown in Figure 44. Figure 45 shows the effect of bioconvection Peclet number  $Pe$  on  $\Omega(\zeta)$  which implies that  $Pe$  increases the microorganisms concentration profile  $\Omega(\zeta)$ . Figure 46 reveals that by increasing the magnetic field parameter  $M$ , the non-dimensional motile density function profile  $\Omega(\zeta)$  is increased.

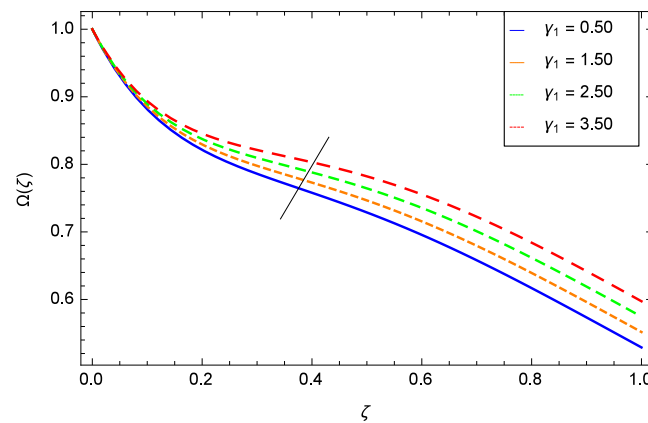


Figure 36: Role of  $\Omega(\zeta)$  and  $\gamma_1$ .

## 5. Conclusions

The present article investigates the MHD mixed convection in gravity-driven non-Newtonian second grade nanofluid flow containing both nanoparticles and gyrotactic microorganisms using Darcy Forchheimer porous medium model of Buongiorno's nanofluid in the presence of chemical reaction along a convectively heated vertical surface. The analytical solution due to Homotopy Analysis Method (HAM) is discussed for the velocity, temperature, concentration and microorganism concentration fields for various parameters. The main findings of the study are the following.

- (i) The velocity  $f(\zeta)$  decreases for the parameters  $\gamma_3, \gamma_4, Rb$  and  $M$  while it increases for the parameters  $\gamma_1, \gamma_2, \gamma_5, Gr, Nr, Le, Sc$  and  $Pr$ .
- (ii) The temperature  $\theta(\zeta)$  decreases for the parameters  $\gamma_2, \gamma_3, \gamma_4, M$  and  $Pr$  while it increases for the parameters  $\gamma_1, \gamma_5$  and  $Nt$ .
- (iii) The concentration  $\phi(\zeta)$  decreases for the parameters  $\gamma_1, \gamma_2, Nt$  and  $Pr$  while it increases for the parameters  $\gamma_3, \gamma_4, \gamma_5, Nb, Le$  and  $M$ .
- (iv) The microorganism concentration  $\Omega(\zeta)$  decreases for the parameters  $\gamma_3, \gamma_4, Nb, Sc$  and  $M$  while it increases for the parameters  $\gamma_1, \gamma_2, \gamma_5, Le, Nt$  and  $Pe$ .

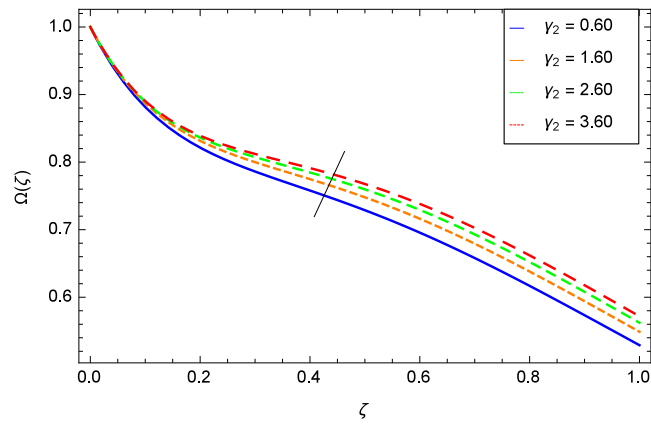


Figure 37: Role of  $\Omega(\zeta)$  and  $\gamma_2$ .

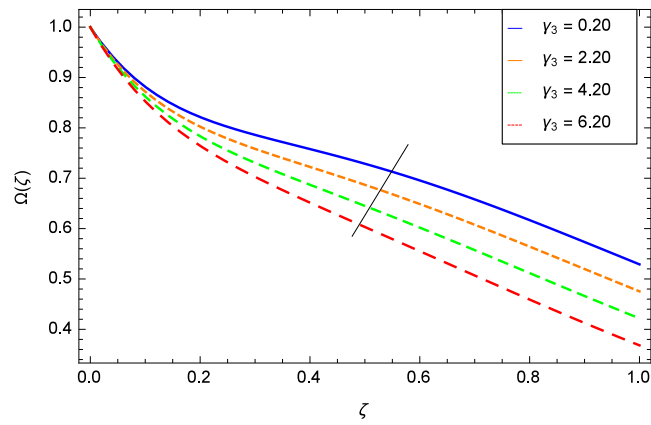


Figure 38: Role of  $\Omega(\zeta)$  and  $\gamma_3$ .

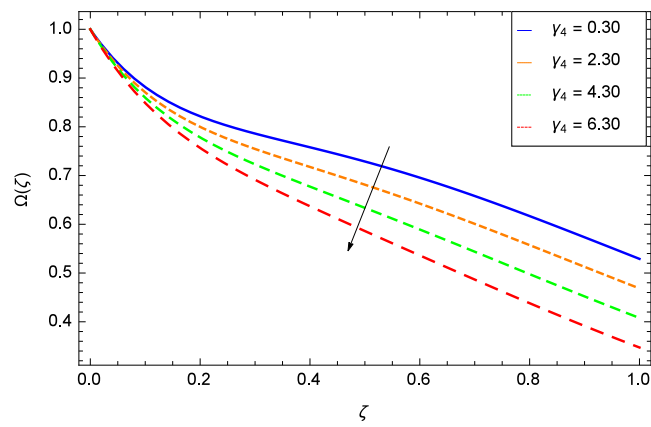


Figure 39: Role of  $\Omega(\zeta)$  and  $\gamma_4$ .

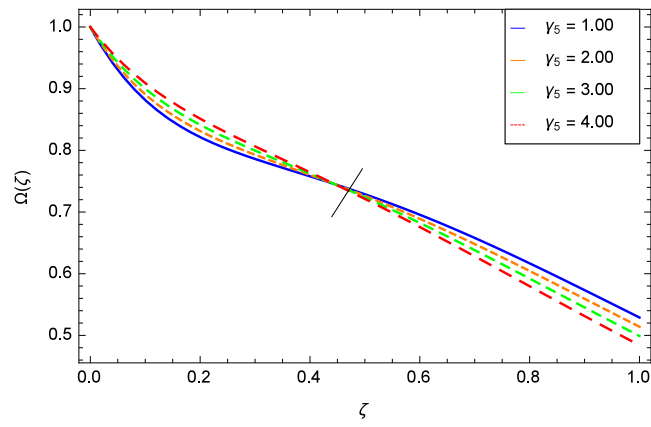


Figure 40: Role of  $\Omega(\zeta)$  and  $\gamma_5$ .

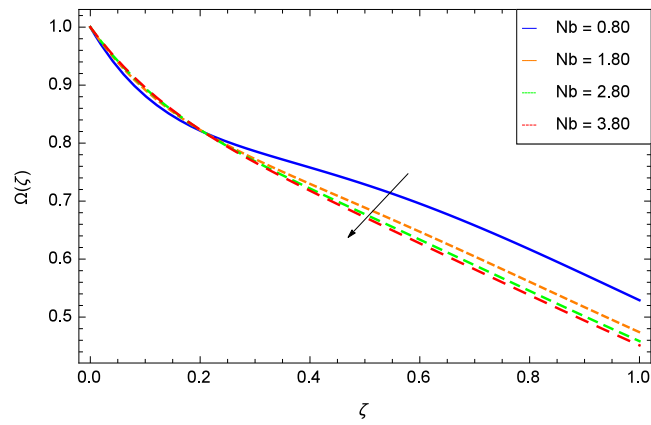


Figure 41: Role of  $\Omega(\zeta)$  and  $Nb$ .

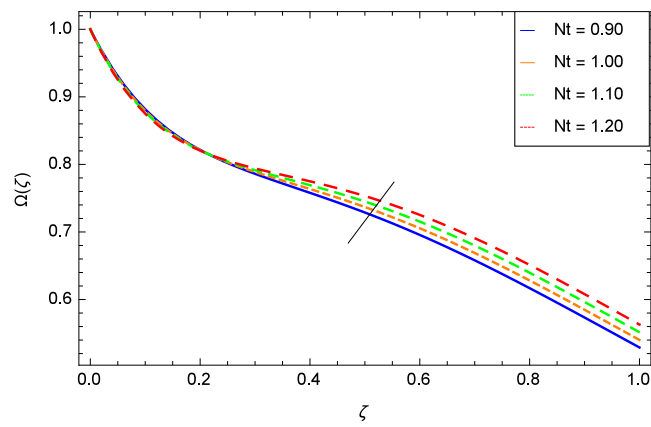


Figure 42: Role of  $\Omega(\zeta)$  and  $Nt$ .

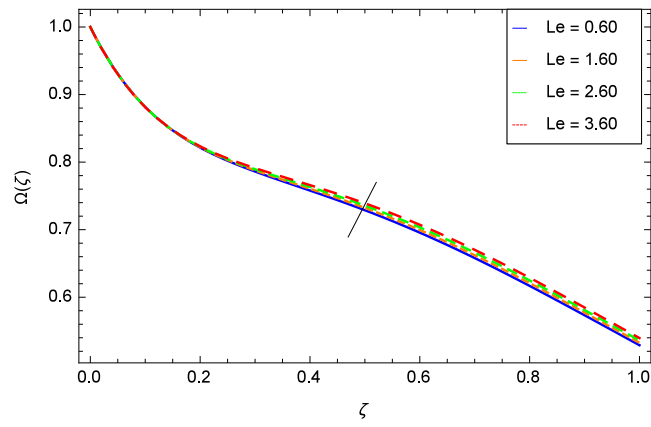


Figure 43: Role of  $\Omega(\zeta)$  and  $Le$ .

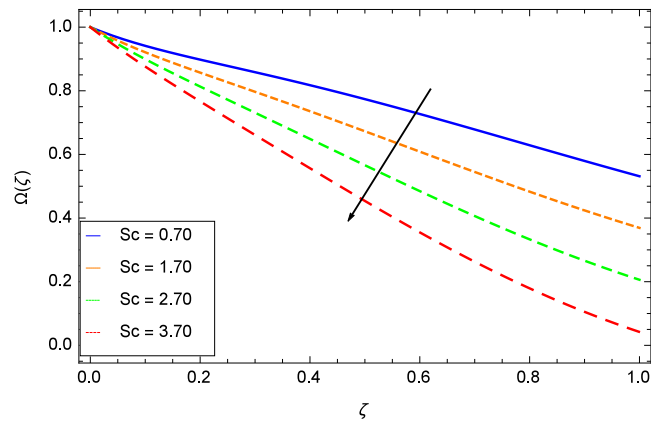


Figure 44: Role of  $\Omega(\zeta)$  and  $Sc$ .

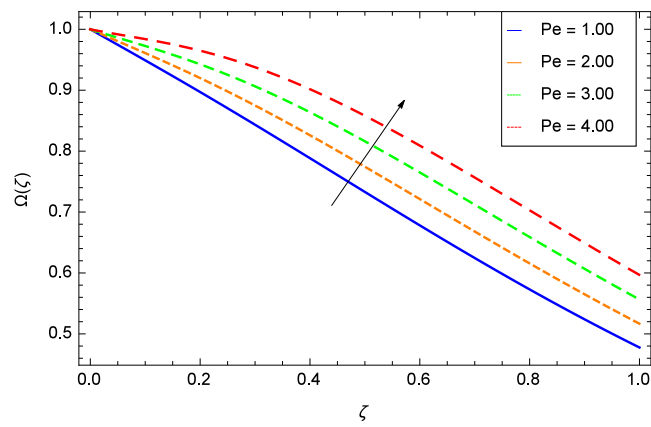
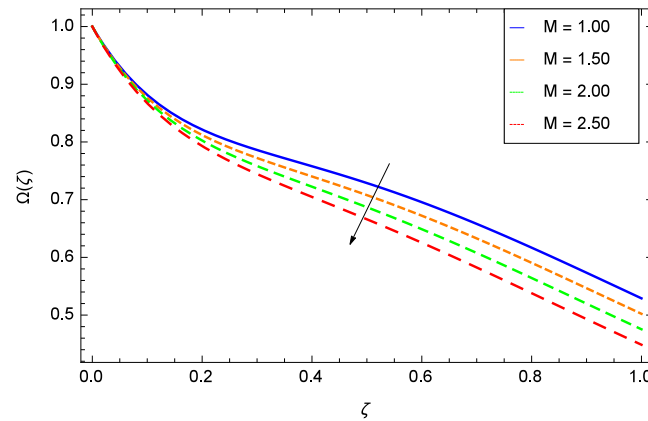


Figure 45: Role of  $\Omega(\zeta)$  and  $Pe$ .

Figure 46: Role of  $\Omega(\zeta)$  and  $M$ .

### Competing Interests

The author declares that he has no competing interests.

### Acknowledgments

The author is thankful to the honorable reviewer for his/her excellent comments and suggestions to improve the quality of the manuscript.

The author is thankful to the Higher Education Commission (HEC) Pakistan for providing the technical and financial support.

### References

- [1] N. S. Khan, T. Gul, M. A. Khan, E. Bonyah, S. Islam, Mixed convection in gravity-driven thin film non-Newtonian nanofluids flow with gyrotactic microorganisms, *Results in Physics* 7 (2017), 4033–4049, <https://dx.doi.org/10.1016/j.rinp.2017.10.017>.
- [2] N. A. Amirsom, M. J. Uddin, Md. F. Md. Basir, A. I. M. Ismail, O. A. Beg, A. Kadir, Three-dimensional bioconvection nanofluid flow from a bi-axial stretching sheet with anisotropic slip, *Sains Malaysiana* 48 (5) (2019) 1137–1149.
- [3] H. Waqas, S. U. Khan, M. Hassan, M. M. Bhatti, M. Imran, Analysis on the bioconvection flow of modified second-grade nanofluid containing gyrotactic microorganisms and nanoparticles, *Journal of Molecular Liquids* 291 (2019) 111231.
- [4] S. U. Khan, A. Rauf, S. A. Hehzad, Z. Abbas, T. Javed, Study of bioconvection flow in Oldroyd-B nanofluid with motile organisms and effective Prandtl approach, *Physica A Statistical Mechanics and its applications*, (2019) 1–31.
- [5] M. A. Mansour, A. M. Rashad, B. Mallikarjuna, A. K. Hussain, M. Aichouni, L. Kolsi, MHD mixed bioconvection in a square porous cavity filled by gyrotactic microorganisms, *International Journal of Heat and Technology*, 37 (2) (2019) 433–445.
- [6] S. Zaman, M. Gul, Magnetohydrodynamic bioconvective flow of Williamson nanofluid containing gyrotactic microorganisms subjected to thermal radiation and Newtonian conditions, *Journal of Theoretical Biology*, 479 (2019) 22–28.
- [7] H. Waqas, S. U. Khan, S. A. Shehzad, M. Imran, Significance of the nonlinear radiative flow of micropolar nanoparticles over porous surface with a gyrotactic microorganisms, activation energy, and Nield's condition, *Heat Transfer Asian Research*, (2019) 1–27.
- [8] M. Ramzan, M. Mohammad, F. Howari, Magnetized suspended carbon nanotubes based nanofluid flow with bio-convection and entropy generation past a vertical cone, *Scientific Reports*, 9 (2019) 12225.
- [9] M. Sohail, R. Naz and S. I. Abdelsalam, On the onset of entropy generation for a nanofluid with thermal radiation and gyrotactic microorganisms through 3D flows, *Physica Scripta* (2019).
- [10] S. Zuhra, N. S. Khan, S. Islam, Magnetohydrodynamic second grade nanofluid flow containing nanoparticles and gyrotactic microorganisms, *Computational and Applied Mathematics* 37 (2018), 6332–6358. <https://dx.doi.org/10.1007/s40314-018-0683-6>.
- [11] S. Zuhra, N. S. Khan, Z. Shah, S. Islam, E. Bonyah, Simulation of bioconvection in the suspension of second grade nanofluid containing nanoparticles and gyrotactic microorganisms. *AIP Advances* 8, (2018) 105210. <https://dx.doi.org/10.1063/1.5054679>.

- [12] N. S. Khan, P. Kumam, P. Thounthong, Renewable energy technology for the sustainable development of thermal system with entropy measures. *International Journal of Heat and Mass Transfer* 145 (2019) 118713. <https://dx.doi.org/10.1016/j.ijheatmasstransfer.2019.118713>.
- [13] Z. Palwasha, S. Islam, N. S. Khan, H. Ayaz, Non-Newtonian nanoliquids thin film flow through a porous medium with magnetotactic microorganisms. *Applied Nanoscience* 8 (2018) 1523–1544. <https://dx.doi.org/10.1007/s13204-018-0834-5>.
- [14] N. S. Khan, Z. Shah, S. Islam, I. Khan, T. A. Alkanhal, I. Tlili, Entropy generation in MHD mixed convection non-Newtonian second-grade nanoliquid thin film flow through a porous medium with chemical reaction and stratification. *Entropy* 21 (2019) 139. <https://dx.doi.org/10.3390/e21020139>.
- [15] N. S. Khan, Bioconvection in second grade nanofluid flow containing nanoparticles and gyrotactic microorganisms. *Brazilian Journal of Physics* 43 (4) (2018) 227–241. <https://dx.doi.org/10.1007/s13538-018-0567-7>.
- [16] A. Anjum, N. A. Mir, M. Farooq, S. Ahmad, N. Rafiq, Optimization of entropy generation in thermally stratified polystyrene-water/kerosene nanofluid flow with convective boundary conditions, *European Physical Journal Plus*, 134 (2019) 176.
- [17] D. Lu, Z. Li, M. Ramzan, A. Shafee, J. D. Chung, Unsteady squeezing carbon nanotubes based nano-liqui flow with Cattaneo-Christov heat flux and homogeneous-heterogeneous reactions, *Applied Nanoscience*, (2018).
- [18] J. Ahmed, M. Khan, L. Ahmad, Stagnation point flow of Maxwell nanofluid over a permeable rotating disk with heat source/sink, *Journal of Molecular Liquids*, (2019).
- [19] C. S. K. Raju, S. U. Mamatha, P. Rajadurai, I. Khan, Nonlinear mixed thermal convective flow over a rotating disk in suspension of magnesium oxide nanoparticles with water and Eg, *European Physical Journal Plus*, 134 (2019) 196.
- [20] N. S. Khan, T. Gul, S. Islam, W. Khan, Thermophoresis and thermal radiation with heat and mass transfer in a magnetohydrodynamic thin film second-grade fluid of variable properties past a stretching sheet. *European Physical Journal Plus*, 132 (2017), <https://dx.doi.org/10.1140/epjp/i2017-11277-3>.
- [21] N. S. Khan, T. Gul, S. Islam, I. Khan, A. M. Alqahtani, A. S. Alshomrani, Magnetohydrodynamic nanoliquid thin film sprayed on a stretching cylinder with heat transfer, *Journal of Applied Sciences*, 7 (2017) 271.
- [22] N. S. Khan, T. Gul, S. Islam, A. Khan, Z. Shah, Brownian motion and thermophoresis effects on MHD mixed convective thin film second-grade nanofluid flow with Hall effect and heat transfer past a stretching sheet, *Journal of Nanofluids*, 6 (2017) 812–829. <https://dx.doi.org/10.1166/jon.2017.1383>.
- [23] N. S. Khan, S. Zuhra, Boundary layer flow and heat transfer in a thin film second-grade nanoliquid embedded with graphene nanoparticles, *Advances in Mechanical Engineering*, 11(11) (2019) 1–11. <https://dx.doi.org/10.1177/1687814019884428>.
- [24] Z. Palwasha, N. S. Khan, Z. Shah, S. Islam, E. Bonyah, Study of two-dimensional boundary layer thin film fluid flow with variable thermophysical-properties in three dimensions space, *AIP Advances* 8 (2018) 105318. <https://dx.doi.org/10.1063/1.5053808>.
- [25] N. S. Khan, S. Zuhra, Z. Shah, E. Bonyah, W. Khan, S. Islam, Slip flow of Eyring-Powell nanoliquid film containing graphene nanoparticles, *AIP Advances* 8 (2019) 115302. <https://dx.doi.org/10.1063/1.5055690>.
- [26] N. S. Khan, S. Zuhra, Q. Shah, Entropy generation in two phase model for simulating flow and heat transfer of carbon nanotubes between rotating stretchable disks with cubic autocatalysis chemical reaction. *Applied Nanoscience* 9 (2019) 1797–1822. <https://dx.doi.org/10.1007/s13204-019-01017-1>.
- [27] S. Zuhra, N. S. Khan, M. A. Khan, S. Islam, W. Khan, E. Bonyah, Flow and heat transfer in water based liquid film fluids dispensed with graphene nanoparticles, *Results in Physics* 8 (2018) 1143–1157. <https://dx.doi.org/10.1016/j.rinp.2018.01.032>.
- [28] N. S. Khan, S. Zuhra, Z. Shah, E. Bonyah, W. Khan, S. Islam, A. Khan, Hall current and thermophoresis effects on magnetohydrodynamic mixed convective heat and mass transfer thin film flow. *Journal of Physics Communication* 3 (2019) 035009. <https://dx.doi.org/10.1088/2399-6528/aa830>
- [29] N. S. Khan, T. Gul, P. Kumam, Z. Shah, S. Islam, W. Khan, S. Zuhra, A. Sohail, Influence of inclined magnetic field on Carreau nanoliquid thin film flow and heat transfer with graphene nanoparticles, *Energies* 12 (2019) 1459. <https://dx.doi.org/10.3390/en12081459>.
- [30] S. Benbernou, A note on the regularity criterion in terms of pressure for the Navier-Stokes equations, *Applied Mathematics Letters*, 22 (2009) 1438–1443.
- [31] S. Gala, Q. Liu, M. A. Ragusa, Logarithmically improved regularity criterion for the nematic liquid crystal flows in  $B_{\infty, \infty}^{-1}$  space, *Computers and Mathematics with Applications*, 65 (2013) 1738–1745.
- [32] S. Gala, Z. Guo, M. A. Ragusa, A remark on the regularity criterion of Boussinesq equations with zero heat conductivity, *Applied Mathematics Letters*, 22 (2014) 70–73.
- [33] N. S. Khan, T. Gul, S. Islam, W. Khan, I. Khan, L. Ali, Thin film flow of a second-grade fluid in a porous medium past a stretching sheet with heat transfer, *Alexandria Engineering Journal* 57 (2017) 1019–1031. <https://dx.doi.org/10.1016/j.aej.2017.01.036>.
- [34] S. Hussain, K. Mehmood, M. Sagheer, A. Ashraf, Mixed convective magnetonanofluid flow over a backward facing step and entropy generation using extended Dary-Brinkman-Forchheimer model, *Journal of Thermal Analysis and Calorimetry* (2019) 1–21.
- [35] G. K. Ramesh, Three different hybrid nanomaterial performances on rotating disk: a non-Darcy model, *Applied Nanoscience*, (2018) 1–9.
- [36] S. Gosh, S. Mukhopadhyay, Stability analysis for model-based study of nanofluid flow over an exponentially shrinking permeable sheet in presence of slip, *Neural Computing and Applications*, (2019) 1–11.
- [37] M. Khan, T. Salahuddin, M. Y. Malik, Implementation of Darcy-Forchheimer effect on magnetohydrodynamic Carreau-Yasuda nanofluid flow: Application of Von Karman, *Canadian Journal of Physics*, (2018) 1–8.
- [38] S. J. Liao, *Homotopy Analysis Method in Nonlinear Differential Equations*, Higher Education Press Beijing and Springer-Verlag Berlin Heidelberg, (2012).